



Chandra Rules Out Super-Eddington Accretion For Little Red Dots

ANDREA SACCHI ¹ AND ÁKOS BOGDÁN ¹¹Center for Astrophysics | Harvard & Smithsonian, 60 Garden Street, Cambridge, MA 20138, USA

ABSTRACT

One of the most puzzling discoveries by JWST is the population of high-redshift, red, and compact galaxies dubbed little red dots (LRDs). Based on broad-line diagnostics, these galaxies have been argued to host accreting $10^7 - 10^8 M_\odot$ supermassive black holes (SMBHs), a claim with crucial consequences for our understanding of how the first black holes form and grow over cosmic time. A key feature of LRDs is their extreme X-ray weakness: analyses of individual and stacked sources have yielded non-detections or only tentative, inconclusive X-ray signals, except for a handful of individual cases. As the most natural explanation, high obscuration, is disfavored by JWST spectroscopic evidence, several authors have suggested that the X-ray weakness of LRDs is intrinsic, due to super-Eddington accretion rates. In this work, we test that scenario by stacking X-ray data for 55 LRDs in the Chandra Deep Field South, accumulating a total exposure time of nearly 400 Ms. Despite reaching unprecedented X-ray depths, our stack still yields a non-detection. The corresponding upper limits are deep enough to rule out current super-Eddington accretion models, and are compatible only with extremely high levels of obscuration ($N_H \gtrsim 10^{25} \text{ cm}^{-2}$). To explain the X-ray weakness of LRDs, we therefore speculate that the SMBHs in these systems are neither as massive nor as luminous as currently believed.

Keywords: supermassive black holes – little red dots – accretion – X-ray active galactic nuclei

1. INTRODUCTION

LRDs are high-redshift compact, red galaxies independently discovered by JWST (Harikane et al. 2023; Koko-rev et al. 2024; Greene et al. 2024; Matthee et al. 2024; Kocevski et al. 2024; Labbe et al. 2025). These galaxies emerge at $z \approx 8$, peak around $z \approx 6$, and rapidly disappears at $z \approx 4$ (Kocevski et al. 2024). The origin of their emission is still debated, with the two main interpretations being either intense star formation (e.g. Baggen et al. 2024) or accretion onto $10^7 - 10^8 M_\odot$ supermassive black holes (SMBHs) (e.g. Kocevski et al. 2023; Greene et al. 2024).

If LRDs host very massive SMBHs (Kocevski et al. 2023; Greene et al. 2024), this has important implications for our understanding of SMBH origins and growth. Such masses imply either that these SMBHs arose from “heavy” seeds (Lodato & Natarajan 2006), or from “light” seeds that grew at super-Eddington rates

(Bromm & Loeb 2003). These SMBHs are also over-massive with respect to their host galaxies. While the masses of SMBHs are about 0.2% of their host galaxies in the local universe (Magorrian et al. 1998; Reines & Volonteri 2015), the mass of SMBHs in LRDs can be as high as 10%–100% of their host galaxies (Harikane et al. 2023; Bogdán et al. 2024; Greene et al. 2024; Kocevski et al. 2024; Kovács et al. 2024).

If LRDs are unobscured AGN with an abundance of $10^{-5} \sim 10^{-4} \text{ Mpc}^{-3} \text{ mag}^{-1}$ at redshift $z \approx 5$ (Greene et al. 2024), their combined X-ray output would be substantial. In fact, if their spectral energy distribution (SED) is the same as local type 1 (unobscured) AGN, their integrated X-ray emission would exceed the observed X-ray background by an order of magnitude (Padmanabhan & Loeb 2023). This issue can be resolved by the X-ray weakness of LRDs. Safe for a handful of sources (Kocevski et al. 2023, 2024), LRDs are not detected in the X-ray band (Kocevski et al. 2024; Matthee et al. 2024), not even when stacking approaches are attempted (Ananna et al. 2024; Maiolino et al. 2025). The only tentative X-ray detection of LRDs, obtained by stacking objects for a total Chandra exposure of ≈ 40 Ms

(Yue et al. 2024), implies optical-to-X-ray ratios that are orders of magnitude above those measured in “typical” AGN (Lusso et al. 2010; Sacchi et al. 2022).

To explain this X-ray weakness, the most natural explanation is heavy obscuration. This, however, requires extremely high column densities ($\log N_{\text{H}} \gtrsim 24$), covering factors approaching 100%, coupled with dust-free environments (Maiolino et al. 2025), which are disfavored by *JWST* spectroscopic evidence. To alleviate this, several authors have proposed that LRDs accrete at super-Eddington rates, resulting in intrinsically X-ray-weak SEDs (Madau & Haardt 2024; Inayoshi et al. 2024; Pacucci & Narayan 2024; Lambrides et al. 2024). In this picture, the lack of X-rays simply reflects the very steep spectral shape compared to more canonical (a few percent Eddington) accretion states.

To test the super-Eddington scenario, we analyze a sample of 55 LRDs with deep available *Chandra* data. *Chandra* is the best-suited instrument to search for faint X-ray emission of high-redshift sources, owing to its unmatched angular resolution and low and stable background. Given that all of the sources we considered lay in the deepest *Chandra* field, i.e. *Chandra* Deep Field South (CDF-S), the total exposure time, stacking the data from all of the considered sources, amounts to ≈ 400 Ms, allowing us to reach unprecedented sensitivity ($\approx 4 \times 10^{-18}$ erg/s/cm²).

Although previous works were able to assess the X-ray weakness of LRDs, they could not reach the sensitivity required to probe the mechanisms at play. Ananna et al. (2024) analyzed *Chandra* data of LRDs lensed by the Abell 2744 cluster. They found that no source is individually detected, and neither is the stacked sample. The authors conclude that, based on the X-ray upper limits they obtained, the masses of the SMBHs hosted in LRDs cannot exceed a few $10^6 M_{\odot}$, assuming a standard unobscured AGN SED accreting at some percent of their Eddington rate. Yue et al. (2024) stacked 34 spectroscopically confirmed LRDs, confirmed their X-ray weakness, and obtained a tentative detection, favoring the AGN interpretation for the emission of LRDs.

The present work surpasses both of these analyses: with respect to Ananna et al. (2024), we can achieve better sensitivity as we do not have to take into account the bright foreground emission of a galaxy cluster; with respect to Yue et al. (2024), we have more objects with much deeper X-ray images, allowing us to account ten times longer total exposure time. Both these works assessed the X-ray weakness of LRDs, and triggered the scientific community to propose different models to explain this feature. Here, exploiting our far more sensitive dataset, we can probe these scenarios.

This paper is organized as follows. In Section 2 we describe our procedure to analyze (stack) the X-ray data; in Section 3 we present our results; in Section 4 we discuss the implications of our X-ray non-detections and discuss the compatibility of our results with current models of X-ray weakness, and we finally draw our conclusions in Section 5. In this work we adopt a flat Λ CDM cosmology with $H_0 = 70$ km/s/Mpc and $\Omega_M = 0.3$.

2. DATA ANALYSIS

2.1. The sample of LRDs

Our parent sample is composed of LRDs identified in the *JWST* Advanced Deep Extragalactic Survey (JADES) (Eisenstein et al. 2023) and the Next Generation Deep Extragalactic Exploratory Public (NGDEEP) (Bagley et al. 2024) surveys by Kocevski et al. (2024). These 56 sources span from redshift $z \approx 3$ to $z \approx 8$, with a mean redshift of $z \approx 6$.

The individual X-ray emission of these sources is discussed in Kocevski et al. (2024). Only one source, JADES 21925, at redshift $z = 3.1$ is X-ray detected, and hence we exclude this source from further analysis. Hereafter, we only address the 55 LRDs that are not individually X-ray detected.

We selected these sources because they lie entirely within the footprint of CDF-S (Giacconi et al. 2002; Luo et al. 2017), which provides the deepest X-ray observation ever taken with *Chandra*, totaling ≈ 7 Ms exposure. Furthermore, most of these observations were taken before 2010, prior to the substantial loss of soft-band sensitivity from the molecular contamination (Plucinsky et al. 2018, 2022).

2.2. X-ray stacking procedure

We downloaded 104 *Chandra* observation of the CDF-S from the *Chandra* data archive¹ and performed the data analysis with the Chandra Interactive Analysis of Observations software package (CIAO, v.4.17 Fruscione et al. 2006) and the CALDB 4.12.0 release of the calibration files. The first step of the analysis was reprocessing the data using `chandra_repro` tool. To improve the absolute astrometry of the merged data, we used the `fine_astro` routine, which cross-matches *Chandra* point sources with other higher precision catalogs, in our case the U. S. Naval Observatory catalog (USNO-A2.0 Monet 1998). The astrometric-corrected and reprojected event files were then merged with the `merge_obs` routine, totaling ≈ 7 Ms of exposure time. The same tool also produced point-spread function (PSF) and exposure maps,

¹ <https://cda.harvard.edu/chaser/mainEntry.do>

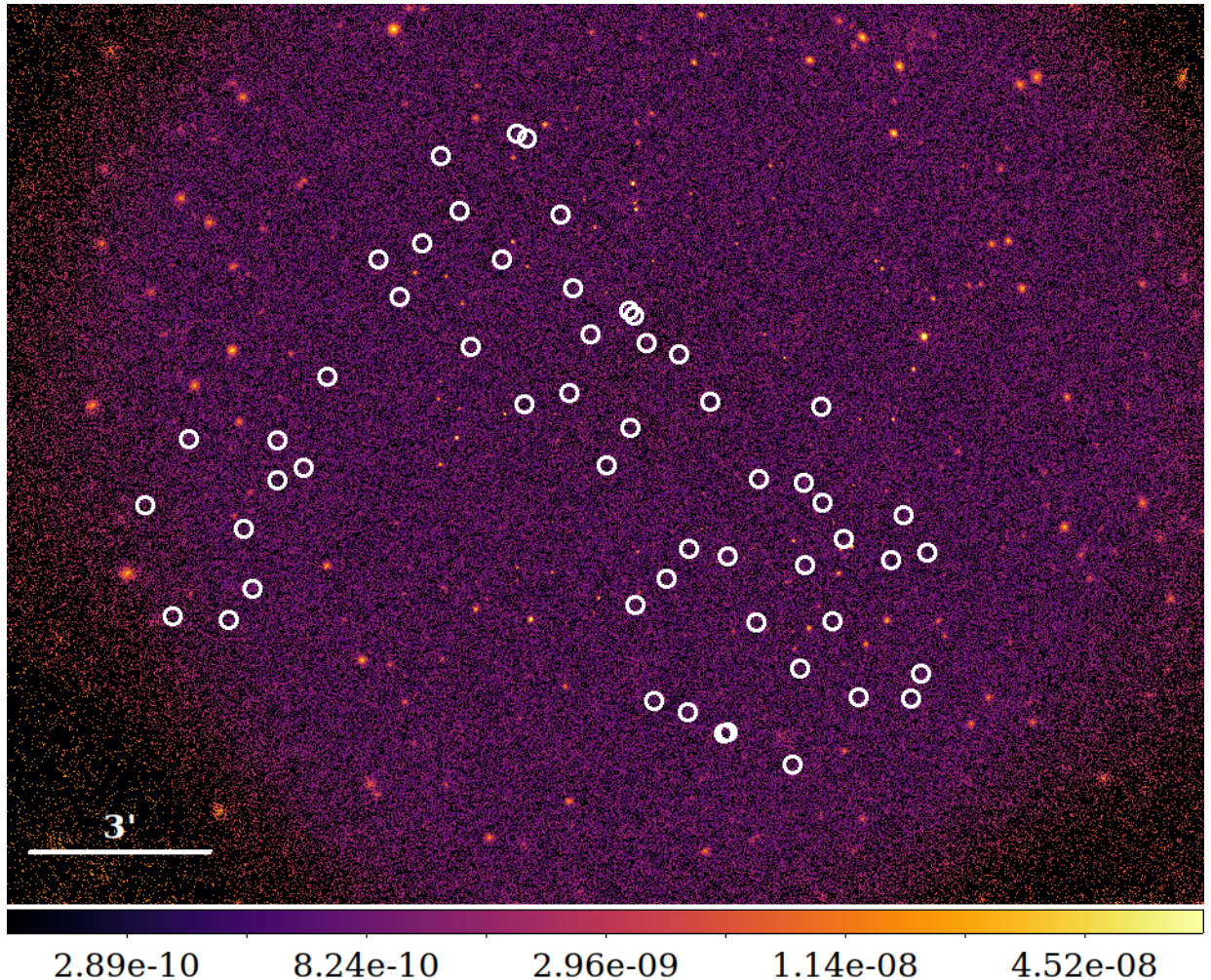


Figure 1. Exposure corrected *Chandra* image in the 0.3 – 7 keV X-ray band of the CDF-S, for which ≈ 7 Ms of total exposure time is available, making it the deepest *Chandra* dataset available to date. The location of each of the 55 LRDs considered in this work is indicated by a white circle with fixed $8''$ radius for illustration purposes.

created assuming a powerlaw spectral profile with photon index $\Gamma = 2$ and line-of-sight Galactic column density $N_{\text{H}} = 6.7 \times 10^{19} \text{ cm}^{-2}$.

Source counts were extracted from circular regions centered on the LRD positions as identified by *JWST*, and background counts from annular regions with the `dmextract` tool. The radius of the extraction region was chosen to correspond to the R_{80} (the radius that includes 80% of the source counts) at the location of each source, and the background regions had radii of $(1.5 - 3)R_{80}$. We note that the choice of adopting R_{80} (instead of the more commonly used R_{90}) does not affect the significance of the (non-)detection, but contributes to lowering the background, in particular for the more off-axis sources. For our 55 sources, the median source extraction region is $R_{80} = 2''$. To avoid contamination from other foreground sources, all point-like sources were identified with the `wavdetect` tool (with wavelet

scales equal to 1.414, 2, 2.828, 4, 5.636, and 8) and accordingly removed. The exposure time for each single source amounts to ≈ 7 Ms, implying that the exposure for the stacked sample amounts to 390 Ms. Figure 1 shows the merged *Chandra* view of CDF-S in the full (0.3 – 7 keV) band with the location of each LRD indicated.

3. RESULTS

By co-adding the X-ray counts across all LRDs, we obtained 1444 (3730) total counts in the soft (0.3 – 2 keV) and hard (2 – 7 keV) band and, after normalizing the background to the same extraction area, we got 1409 (3697) background counts in the soft and hard bands, respectively. This yields 35 ± 41 net counts in the soft band and 33 ± 66 in the hard band, corresponding to non-detections. In the absence of detections, we derive upper limits on the flux of the stacked LRD population. To this end, we adopt the exposure maps and

convert the count rates into fluxes, obtaining 3σ upper limits of $< 4.7 \times 10^{-18}$ erg/s/cm² in the soft and $< 1.3 \times 10^{-17}$ erg/s/cm² in the hard band. We note that the choice of photon index adopted to convert the count rates into fluxes affects these latter by only $\approx 20\%$, leaving our main results unchanged.

We convert our flux limits into bolometric luminosities by adopting standard bolometric corrections ($L_{\text{bol}}/L_X = 16.7$, Lusso et al. 2012; Duras et al. 2020). We obtain an upper limit of $L_{\text{bol}} < 3 \times 10^{43}$ erg/s, which is more than an order of magnitude lower than the average bolometric luminosities of LRDs inferred from *JWST* observations ($L_{\text{bol}} \approx 5 \times 10^{44}$ erg/s, Harikane et al. 2023; Kocevski et al. 2024).

Our results are in line with those obtained by previous works: stacking the X-ray data of individually non-detected LRDs results in a non-detection (Ananna et al. 2024; Maiolino et al. 2025). However, we do not confirm the tentative detection of Yue et al. (2024).

4. DISCUSSION

Here we discuss possible explanations for the extreme X-ray weakness we inferred for the LRDs in our sample. We discuss three potential scenarios:

- The sample may include non-AGN contaminants, hence the signal from the accreting SMBHs is diluted by the presence of spurious sources;
- The SED of the LRDs is that of a standard type 1 AGN, but the X-ray emission is heavily obscured;
- The SED of the LRDs is not that of standard type 1 AGN and their X-ray emission is intrinsically weak.

4.1. Non-AGN contaminants

Some of the objects in our sample could be high-redshift galaxies without active SMBH accretion, or foreground interlopers such as brown dwarfs. However, to explain the lack of X-ray emission of LRDs invoking uniquely non-AGN contaminants, one needs to assume that the majority of the considered objects are spurious sources (Maiolino et al. 2025). This scenario has already been ruled out by *JWST* spectroscopic follow-ups of early compilations of LRD samples, which confirmed the presence of broad H_α emission lines for most of them, reinforcing the AGN interpretation (Kocevski et al. 2023). Greene et al. (2024) followed up photometrically-selected LRDs and found that $\approx 60\%$ show broad H_α emission lines, for a small fraction ($\approx 20\%$) the line diagnostic was inconclusive, and a final $\approx 20\%$ was non-AGN contaminants, i.e. brown dwarfs.

Our sample of LRDs, however, was carefully selected to avoid the presence of such objects based on their infrared colors (Kocevski et al. 2024), hence we do not expect this last fraction to be as significant. Nonetheless, in the rest of the discussion, we contemplate the possibility that 20% of the sources may be non-AGN contaminants.

4.2. High obscuration

High column densities could be responsible for the X-ray weakness of LRDs. As already argued in previous studies (Ananna et al. 2024; Maiolino et al. 2025), to hide the X-ray emission at the measured levels, column densities in excess of 10^{24} cm⁻² are needed, implying a Compton-thick regime. Residual X-ray emission is expected from reflection on the material surrounding and obscuring the SMBHs. This scenario needs further tuning to account for the multi-wavelength features of LRDs (e.g. the absence of dust and the presence of broad emission lines Maiolino et al. 2025), but a discussion of these aspects is beyond the scope of this work: here we focus on the X-ray emission itself. To test if Compton-thickness is compatible with the deep *Chandra* upper limits derived from our stacking analysis (Section 3), we compare these with mock spectra of Compton-thick AGN with different values of column densities. The mock spectra were created with the *borus02* model (Baloković et al. 2019). The normalization of the transmitted component was set assuming a bolometric luminosity of $L_{\text{bol}} = 5 \times 10^{44}$ erg/s, and the standard bolometric correction of $k_{\text{bol}} = 16.7$ (Duras et al. 2020). We assumed a covering factor $CF = 1$ and an inclination angle $\cos \theta = 0.05$. The model is also shifted to the mean redshift of our sample. Figure 2 shows the comparison between the mock spectra and the upper limits we derived. The solid red lines correspond to column densities of $N_H = 10^{24.5-25}$ cm⁻². When compared to the *Chandra* upper limits, reported in black, one can see that only extremely high values of column densities $N_H \gtrsim 10^{25}$ cm⁻² are permitted. Such high values of N_H are in contrast with the results of *JWST* high-resolution spectroscopy, and cannot be reconciled by assuming that $\approx 20\%$ of the sources in our sample are spurious (but see Maiolino et al. 2025 for possible ways to reconcile the two results).

4.3. Intrinsic X-ray weakness

Intrinsic X-ray weakness, motivated by accretion rates at, or even exceeding, the Eddington limit, has been invoked by multiple authors to explain the X-ray non-detections of LRDs (Inayoshi et al. 2024; Madau & Haardt 2024; Lambrides et al. 2024; Pacucci & Narayan

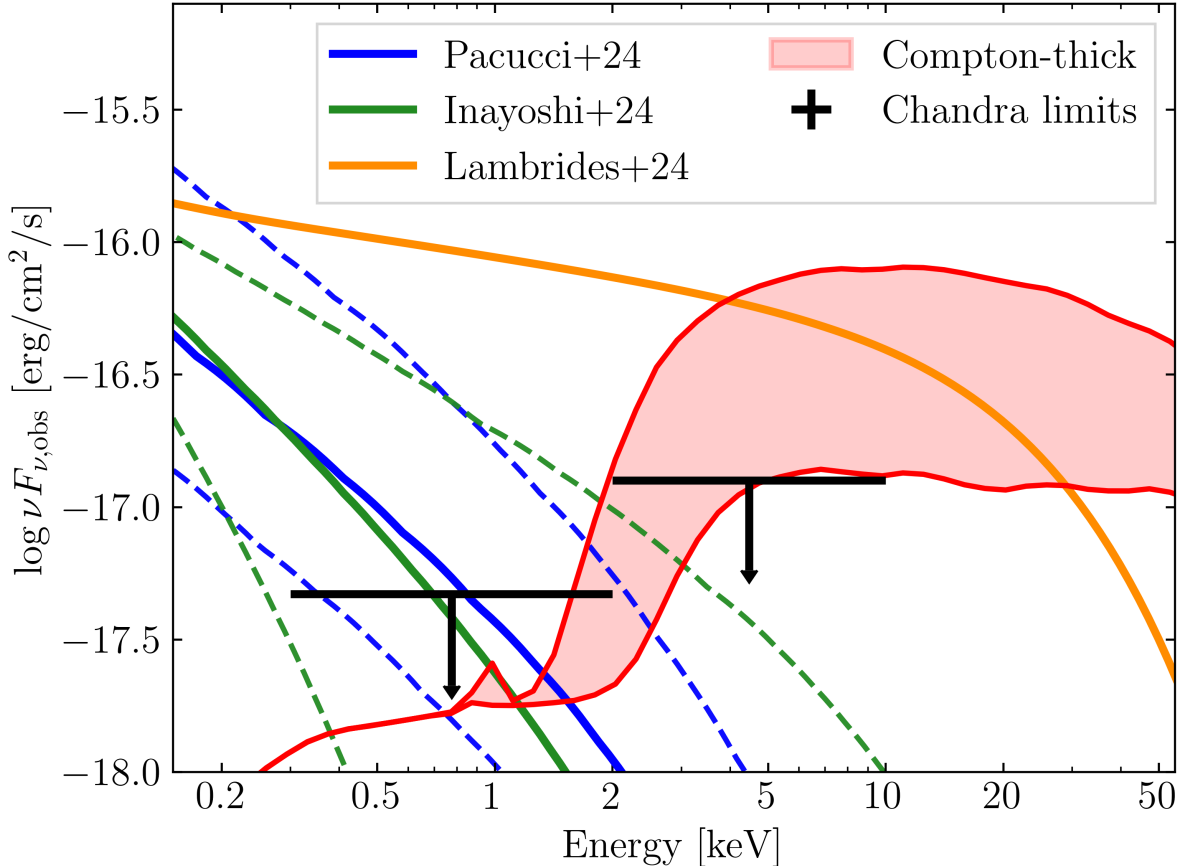


Figure 2. Comparison between the upper limits on the X-ray emission of LRDs derived in this work and mock spectra corresponding to different scenarios of X-ray weakness. Intrinsic X-ray weakness from super-Eddington accretion from [Pacucci & Narayan \(2024\)](#) and [Inayoshi et al. \(2024\)](#) are reported in blue and green, respectively. For [Pacucci & Narayan \(2024\)](#), the solid line indicates the mean expected flux, the dashed lines encompass a region spanning the viewing angles range $\theta = 30^\circ - 80^\circ$. For [Inayoshi et al. \(2024\)](#), the solid line indicates an Eddington ratio $\lambda_{\text{Edd}} = 1$, and the dashed lines encompass a region which spans the range of Eddington ratios $\lambda_{\text{Edd}} = 0.3 - 3$. In orange is shown the model for super-Eddington accretion `agnslim`, assumed by [Lambrides et al. \(2024\)](#). In red is shown a standard Compton-thick spectrum (`borus02`, [Baloković et al. 2019](#)), the solid lines corresponding to column densities of $N_{\text{H}} = 10^{24.5-25} \text{ cm}^{-2}$.

2024; Naidu et al. 2025). Indeed, in the local universe, the AGN accreting at high fractions of their Eddington rates usually exhibit softer and less luminous X-ray emission ([Tortosa et al. 2023](#)).

As prototypes for super-Eddington accretion models, we adopt the spectral profiles presented by [Pacucci & Narayan \(2024\)](#) and [Inayoshi et al. \(2024\)](#). Using general relativistic radiation magnetohydrodynamics (GR-RMHD) simulations, [Pacucci & Narayan \(2024\)](#) obtained a family of X-ray spectral profiles of SMBHs accreting at super-Eddington rates, observed at different viewing angles. [Inayoshi et al. \(2024\)](#) performed a similar exercise via an analytical approach, spanning different mass accretion rates.

Both families of spectra have bolometric luminosities compatible with those inferred for LRDs, and we red-

shifted them to the mean redshift of the sources in our sample ($z = 6$). We adopted the models presented in Fig. 4 (bottom-left panel) of [Pacucci & Narayan \(2024\)](#), corresponding the X-ray weak case, and in Fig. 3 (left panel) of [Inayoshi et al. \(2024\)](#), corresponding to the case of an AGN powered by accretion onto a $10^7 M_\odot$ SMBH.

In Fig. 2, we compare these two models with our upper limits. In blue is the model by [Pacucci & Narayan \(2024\)](#): the dashed lines encompass a region which spans the range of viewing angles $\theta = 30^\circ - 80^\circ$, and the solid line indicates the average spectrum. In green is the family of SEDs derived by [Inayoshi et al. \(2024\)](#): the dashed lines encompass a region corresponding to a range of Eddington rates $\lambda_{\text{Edd}} = 0.3 - 3$ and the solid line indicates $\lambda_{\text{Edd}} = 1$ (λ_{Edd} is mass accretion rate in units

of Eddington rate). Both models, although derived in different and independent ways, show similar profiles. This is a common trait for super-Eddington accretion models; they all predict extremely soft X-ray emission. Indeed, when parametrized with a power law profile, typical photon indices are $\Gamma \gtrsim 3$.

As is clear from Fig. 2, none of these models are compatible with the *Chandra* upper limits we derived for our sample. For the Pacucci & Narayan (2024) models, not only is the average spectrum ruled out, but even the most extreme viewing angles. Even in the unlikely scenario in which all of the SMBHs hosted in LRDs are seen edge-on, the resulting X-ray emission would be detected by *Chandra* with a $> 3\sigma$ significance. For Inayoshi et al. (2024), only the most extreme values of accretion rate are not ruled out ($\lambda_{\text{Edd}} \gtrsim 3$), as the spectrum is so steep that it falls outside the soft X-ray band.

Finally, even assuming that only 80% of the LRDs in our sample actually host an accreting SMBH, it would not introduce a sufficiently large correction to reconcile the examined model with the *Chandra* upper limits.

The super-Eddington SEDs presented here represent excellent prototypes for this family of models, and our conclusions also extend to those proposed by other authors, as all of them predict similar X-ray slopes and luminosities. For completeness, in Fig. 2 we also show (in orange) the super-Eddington accretion model adopted by Lambrides et al. (2024). These authors did not derive an SED, but assumed one to provide seed photons to a photo-ionization model to reproduce the emission lines observed in LRDs spectra. The model assumed for super-Eddington accretion is a slim disk spectrum (agnslim, Kubota & Done 2019), that we set to have the same parameters as those described by Lambrides et al. (2024). The presence of a warm corona in this model, in addition to a slim accretion disk, generates a considerable amount of X-ray emission, exceeding by 1 – 1.5 orders of magnitude the upper limits we derived, and it is hence ruled out.

Based on this evidence, we conclude that present *Chandra* observations rule out current super-Eddington accretion models that aim to explain the X-ray weakness of LRDs.

4.4. Overestimated masses and bolometric luminosities

Based on the evidence reported so far, *Chandra* data rule current models of super-Eddington accretion, and are compatible only with extremely high levels of obscuration (disfavored by *JWST* spectroscopy). To reconcile the X-ray upper limits with our current understanding of accretion onto SMBHs, it has been argued that the masses of the SMBHs hosted in LRDs are overestimated

(Ananna et al. 2024; Maiolino et al. 2025; Rusakov et al. 2025). However, this alone cannot solve the puzzle of the multi-wavelength behavior of LRDs, as the proposed models are normalized on the bolometric luminosities rather than on the SMBHs masses. Hence, lowering the masses of the SMBHs will not affect the normalization of the models, but will simply increase the inferred accretion rates.

As full (multi-wavelength) SED-modeling for LRDs is not feasible, bolometric luminosities are inferred either from the luminosities of the broad H_α line or of the rest-frame optical/UV continuum, exploiting empirical relations derived from local unobscured AGN (e.g. Stern & Laor 2012). We argue that the underlying assumption that LRDs share the same SED of local unobscured AGN is fundamentally disproved by their X-ray weakness, and we conclude that the bolometric luminosities are overestimated.

If we assume lower bolometric luminosities, more modest column densities would be sufficient to obscure the X-ray emission from LRDs, with no need to invoke super-Eddington accretion. Although reducing the bolometric luminosities, and hence the SMBH masses, would make super-Eddington models compatible with our X-ray upper limits, such models would be unnecessary as standard accretion regimes could fully explain the observed X-ray properties.

5. CONCLUSIONS

In this work we explored the X-ray properties of 55 LRDs identified in the JADES and NGDEEP surveys. These objects are not individually X-ray detected, and also by stacking all of them, we obtained a non-detection, both in the soft and hard X-ray band. This result falls in line with those obtained by exploiting different datasets, but the 3σ upper limits we derived, based on a total exposure time of ≈ 390 Ms, are the deepest ever obtained.

Leveraging this unprecedented sensitivity, we tested super-Eddington accretion models proposed to explain the X-ray weakness of LRDs. None of these models is compatible with our observations, ruling out super-Eddington accretion. Furthermore, since non-AGN contaminants are expected to be negligible, our X-ray results require extreme Compton thickness, which is also ruled out by *JWST* spectroscopy.

To relax this tension, we argue that both the bolometric luminosities and SMBH masses are overestimated, which has been suggested by several authors. If the bolometric luminosities are overestimated by an order of magnitude, much lower levels of obscuration can hide

the X-ray emission from accreting SMBHs without invoking super-Eddington accretion.

ACKNOWLEDGMENTS

Á.B. acknowledges support from the Smithsonian Institution and the Chandra Project through NASA contract NAS8-03060. This research has made use of data obtained from the Chandra Data Archive and the Chan-

dra Source Catalog, both provided by the Chandra X-ray Center (CXC). This paper employs a list of Chandra data sets, obtained by the Chandra X-ray Observatory, available at DOI: [10.25574/cdc.382](https://doi.org/10.25574/cdc.382).

Facility: CXO

Software: Astropy (Astropy Collaboration et al. 2013, 2018), Matplotlib (Hunter 2007), NumPy (Harris et al. 2020), Ds9

REFERENCES

- Ananna, T. T., Bogdán, Á., Kovács, O. E., Natarajan, P., & Hickox, R. C. 2024, ApJL, 969, L18, doi: [10.3847/2041-8213/ad5669](https://doi.org/10.3847/2041-8213/ad5669)
- Astropy Collaboration, Robitaille, T. P., Tollerud, E. J., et al. 2013, A&A, 558, A33, doi: [10.1051/0004-6361/201322068](https://doi.org/10.1051/0004-6361/201322068)
- Astropy Collaboration, Price-Whelan, A. M., Sipőcz, B. M., et al. 2018, AJ, 156, 123, doi: [10.3847/1538-3881/aabc4f](https://doi.org/10.3847/1538-3881/aabc4f)
- Baggen, J. F. W., van Dokkum, P., Brammer, G., et al. 2024, ApJL, 977, L13, doi: [10.3847/2041-8213/ad90b8](https://doi.org/10.3847/2041-8213/ad90b8)
- Bagley, M. B., Pirzkal, N., Finkelstein, S. L., et al. 2024, ApJL, 965, L6, doi: [10.3847/2041-8213/ad2f31](https://doi.org/10.3847/2041-8213/ad2f31)
- Baloković, M., García, J. A., & Cabral, S. E. 2019, Research Notes of the American Astronomical Society, 3, 173, doi: [10.3847/2515-5172/ab578e](https://doi.org/10.3847/2515-5172/ab578e)
- Bogdán, Á., Goulding, A. D., Natarajan, P., et al. 2024, Nature Astronomy, 8, 126, doi: [10.1038/s41550-023-02111-9](https://doi.org/10.1038/s41550-023-02111-9)
- Bromm, V., & Loeb, A. 2003, ApJ, 596, 34, doi: [10.1086/377529](https://doi.org/10.1086/377529)
- Duras, F., Bongiorno, A., Ricci, F., et al. 2020, A&A, 636, A73, doi: [10.1051/0004-6361/201936817](https://doi.org/10.1051/0004-6361/201936817)
- Eisenstein, D. J., Johnson, B. D., Robertson, B., et al. 2023, arXiv e-prints, arXiv:2310.12340, doi: [10.48550/arXiv.2310.12340](https://doi.org/10.48550/arXiv.2310.12340)
- Fruscione, A., McDowell, J. C., Allen, G. E., et al. 2006, in Society of Photo-Optical Instrumentation Engineers (SPIE) Conference Series, Vol. 6270, Observatory Operations: Strategies, Processes, and Systems, ed. D. R. Silva & R. E. Doxsey, 62701V, doi: [10.1117/12.671760](https://doi.org/10.1117/12.671760)
- Giacconi, R., Zirm, A., Wang, J., et al. 2002, ApJS, 139, 369, doi: [10.1086/338927](https://doi.org/10.1086/338927)
- Greene, J. E., Labbe, I., Goulding, A. D., et al. 2024, ApJ, 964, 39, doi: [10.3847/1538-4357/ad1e5f](https://doi.org/10.3847/1538-4357/ad1e5f)
- Harikane, Y., Zhang, Y., Nakajima, K., et al. 2023, ApJ, 959, 39, doi: [10.3847/1538-4357/ad029e](https://doi.org/10.3847/1538-4357/ad029e)
- Harris, C. R., Millman, K. J., van der Walt, S. J., et al. 2020, Nature, 585, 357, doi: [10.1038/s41586-020-2649-2](https://doi.org/10.1038/s41586-020-2649-2)
- Hunter, J. D. 2007, Computing in Science and Engineering, 9, 90, doi: [10.1109/MCSE.2007.55](https://doi.org/10.1109/MCSE.2007.55)
- Inayoshi, K., Kimura, S., & Noda, H. 2024, arXiv e-prints, arXiv:2412.03653, doi: [10.48550/arXiv.2412.03653](https://doi.org/10.48550/arXiv.2412.03653)
- Kocevski, D. D., Onoue, M., Inayoshi, K., et al. 2023, ApJL, 954, L4, doi: [10.3847/2041-8213/ace5a0](https://doi.org/10.3847/2041-8213/ace5a0)
- Kocevski, D. D., Finkelstein, S. L., Barro, G., et al. 2024, arXiv e-prints, arXiv:2404.03576, doi: [10.48550/arXiv.2404.03576](https://doi.org/10.48550/arXiv.2404.03576)
- Kokorev, V., Caputi, K. I., Greene, J. E., et al. 2024, ApJ, 968, 38, doi: [10.3847/1538-4357/ad4265](https://doi.org/10.3847/1538-4357/ad4265)
- Kovács, O. E., Bogdán, Á., Natarajan, P., et al. 2024, ApJL, 965, L21, doi: [10.3847/2041-8213/ad391f](https://doi.org/10.3847/2041-8213/ad391f)
- Kubota, A., & Done, C. 2019, MNRAS, 489, 524, doi: [10.1093/mnras/stz2140](https://doi.org/10.1093/mnras/stz2140)
- Labbe, I., Greene, J. E., Bezanson, R., et al. 2025, ApJ, 978, 92, doi: [10.3847/1538-4357/ad3551](https://doi.org/10.3847/1538-4357/ad3551)
- Lambrides, E., Garofali, K., Larson, R., et al. 2024, arXiv e-prints, arXiv:2409.13047, doi: [10.48550/arXiv.2409.13047](https://doi.org/10.48550/arXiv.2409.13047)
- Lodato, G., & Natarajan, P. 2006, MNRAS, 371, 1813, doi: [10.1111/j.1365-2966.2006.10801.x](https://doi.org/10.1111/j.1365-2966.2006.10801.x)
- Luo, B., Brandt, W. N., Xue, Y. Q., et al. 2017, ApJS, 228, 2, doi: [10.3847/1538-4365/228/1/2](https://doi.org/10.3847/1538-4365/228/1/2)
- Lusso, E., Comastri, A., Vignali, C., et al. 2010, A&A, 512, A34, doi: [10.1051/0004-6361/200913298](https://doi.org/10.1051/0004-6361/200913298)
- Lusso, E., Comastri, A., Simmons, B. D., et al. 2012, MNRAS, 425, 623, doi: [10.1111/j.1365-2966.2012.21513.x](https://doi.org/10.1111/j.1365-2966.2012.21513.x)
- Madau, P., & Haardt, F. 2024, ApJL, 976, L24, doi: [10.3847/2041-8213/ad90e1](https://doi.org/10.3847/2041-8213/ad90e1)
- Magorrian, J., Tremaine, S., Richstone, D., et al. 1998, AJ, 115, 2285, doi: [10.1086/300353](https://doi.org/10.1086/300353)
- Maiolino, R., Risaliti, G., Signorini, M., et al. 2025, MNRAS, 538, 1921, doi: [10.1093/mnras/staf359](https://doi.org/10.1093/mnras/staf359)

- Matthee, J., Naidu, R. P., Brammer, G., et al. 2024, *ApJ*, 963, 129, doi: [10.3847/1538-4357/ad2345](https://doi.org/10.3847/1538-4357/ad2345)
- Monet, D. 1998, USNO-A2.0
- Naidu, R. P., Matthee, J., Katz, H., et al. 2025, arXiv e-prints, arXiv:2503.16596, doi: [10.48550/arXiv.2503.16596](https://doi.org/10.48550/arXiv.2503.16596)
- Pacucci, F., & Narayan, R. 2024, *ApJ*, 976, 96, doi: [10.3847/1538-4357/ad84f7](https://doi.org/10.3847/1538-4357/ad84f7)
- Padmanabhan, H., & Loeb, A. 2023, *ApJL*, 958, L7, doi: [10.3847/2041-8213/ad09ac](https://doi.org/10.3847/2041-8213/ad09ac)
- Plucinsky, P. P., Bogdan, A., & Marshall, H. L. 2022, in Society of Photo-Optical Instrumentation Engineers (SPIE) Conference Series, Vol. 12181, Space Telescopes and Instrumentation 2022: Ultraviolet to Gamma Ray, ed. J.-W. A. den Herder, S. Nikzad, & K. Nakazawa, 121816X, doi: [10.1117/12.2630193](https://doi.org/10.1117/12.2630193)
- Plucinsky, P. P., Bogdan, A., Marshall, H. L., & Tice, N. W. 2018, in Society of Photo-Optical Instrumentation Engineers (SPIE) Conference Series, Vol. 10699, Space Telescopes and Instrumentation 2018: Ultraviolet to Gamma Ray, ed. J.-W. A. den Herder, S. Nikzad, & K. Nakazawa, 106996B, doi: [10.1117/12.2312748](https://doi.org/10.1117/12.2312748)
- Reines, A. E., & Volonteri, M. 2015, *ApJ*, 813, 82, doi: [10.1088/0004-637X/813/2/82](https://doi.org/10.1088/0004-637X/813/2/82)
- Rusakov, V., Watson, D., Nikopoulos, G. P., et al. 2025, arXiv e-prints, arXiv:2503.16595, doi: [10.48550/arXiv.2503.16595](https://doi.org/10.48550/arXiv.2503.16595)
- Sacchi, A., Risaliti, G., Signorini, M., et al. 2022, *A&A*, 663, L7, doi: [10.1051/0004-6361/202243411](https://doi.org/10.1051/0004-6361/202243411)
- Stern, J., & Laor, A. 2012, *MNRAS*, 423, 600, doi: [10.1111/j.1365-2966.2012.20901.x](https://doi.org/10.1111/j.1365-2966.2012.20901.x)
- Tortosa, A., Ricci, C., Ho, L. C., et al. 2023, *MNRAS*, 519, 6267, doi: [10.1093/mnras/stac3590](https://doi.org/10.1093/mnras/stac3590)
- Yue, M., Eilers, A.-C., Ananna, T. T., et al. 2024, *ApJL*, 974, L26, doi: [10.3847/2041-8213/ad7eba](https://doi.org/10.3847/2041-8213/ad7eba)